Physica A 468 (2017) 267–277

Contents lists available at ScienceDirect

Physica A

journal homepage: www.elsevier.com/locate/physa

A quantum relativistic battle of the sexes cellular automaton

Ramón Alonso-Sanz [a,*], Haozhen Situ [b]

[a] Technical University of Madrid, ETSIA (Estadística, GSC). C.Universitaria, Madrid 28040, Spain
[b] College of Mathematics and Informatics, South China Agricultural University, Guangzhou 510642, China

HIGHLIGHTS

- This work deals with a spatial formulation of the iterated quantum-relativistic battle of the sexes (QRBOS) game played in the cellular automata (CA) manner.
- The parameters of the model are quickly selected and promptly converge to a fairly stable structure.
- In fair two-parameter games, the simulations evolve into parameter structures that favour the accelerated players when the entanglement factor γ lies below its midpoint, and to the inertial ones above it.
- Quantum-accelerated players become fully privileged when facing classic-inertial ones regardless γ.
- Classic-accelerated players overrate the quantum-inertial ones with γ under its midpoint, whereas the payoffs order reverses with γ over its midpoint.
- In the three-parameter model, the accelerated players overrate the inertial ones up to a high level of γ, above which the payoffs of both player types tend to equalize.
- Heavy spatial effects emerge in CA simulations with no negligible γ, so that mean-field payoff estimates fail to approach to the actual mean payoffs.

ARTICLE INFO

Article history:
Received 15 July 2016
Received in revised form 31 October 2016
Available online 14 November 2016

Keywords:
Quantum games
Entangling
Uniform acceleration
Cellular automata

ABSTRACT

The effect of variable entangling on the dynamics of a spatial quantum relativistic formulation of the iterated battle of the sexes game is studied in this work. The game is played in the cellular automata manner, i.e., with local and synchronous interaction. The game is assessed in fair and unfair contests. Despite the full range of quantum parameters initially accessible, they promptly converge into fairly stable configurations, that often show rich spatial structures in simulations with no negligible entanglement.

1. The classic, quantum, and quantum relativistic BOS

The so called *battle of the sexes* (BOS) is a simple example of a two-person (A, B or ♂, ♀), non-zero sum asymmetric game, i.e., a game whose payoff matrices are not coincident after transposition. Thus, for example: $\mathbf{P}_{♂} = \begin{pmatrix} R & 0 \\ 0 & \varrho \end{pmatrix}$, and $\mathbf{P}_{♀} = \begin{pmatrix} \varrho & 0 \\ 0 & R \end{pmatrix}$. The rewards $R > \varrho > 0$ quantify the preferences in a conventional couple fitting the traditional stereotypes: The male prefers to attend a *F*ootball match, whereas the female prefers to attend a *B*allet performance. Both players hope to *coordinate* their choices, but the *conflict* is also present because their preferred activities differ [1].

* Corresponding author.
E-mail addresses: ramon.alonso@upm.es (R. Alonso-Sanz), situhaozhen@gmail.com (H. Situ).

http://dx.doi.org/10.1016/j.physa.2016.11.003
0378-4371/

1.1. The classic context

In the conventional classic context both players use uncorrelated probabilistic strategies $\mathbf{x} = (x, 1-x)', \mathbf{y} = (y, 1-y)'$, achieving the expected payoffs (p):

$$p_{\male}(x; y) = \mathbf{x}'\mathbf{P}_{\male}\mathbf{y}, \qquad p_{\female}(y; x) = \mathbf{x}'\mathbf{P}_{\female}\mathbf{y}. \tag{1}$$

The pair of strategies ($\mathbf{x}$, $\mathbf{y}$) are in Nash equilibrium (NE) if neither player can improve their payoff by a unilateral change in strategy. The three NE in the BOS are: $x = y = 0, x = y = 1$, and $\big(x = R/(R+\varrho), y = 1-x\big)$. Both players get the same payoff if $y = 1-x$, with maximum $p^+ = (R+\varrho)/4$ for $x = y = 1/2$.

In a different game scenario, usually referred to as *correlated* games, the players have not an active role, instead of it an *external* probability distribution $\mathbf{\Pi}$ assigns probability to every combination of player choices, so $\mathbf{\Pi} = \binom{\pi_{11}\ \ \pi_{12}}{\pi_{21}\ \ \pi_{22}}$ in 2×2 games [1]. Thus, the expected payoffs in the BOS are given by:

$$p_{\begin{Bmatrix}\male\\ \female\end{Bmatrix}} = \begin{Bmatrix}R\\ \varrho\end{Bmatrix}\pi_{11} + \begin{Bmatrix}\varrho\\ R\end{Bmatrix}\pi_{22}. \tag{2}$$

If $\pi_{11} = \pi_{22} = \pi$, both players get the same payoff $p^= = \pi(R+\varrho)$, which if $\pi > 1/4$ is not accessible with independent players; with maximum $p^+ = (R+\varrho)/2$ if $\pi = 1/2$.

The quantum model described in the next subsection, includes both the independent players model (1), and that of the $\mathbf{\Pi}$-correlated games [2].

1.2. Quantum games

In the quantization scheme introduced by Eisert et al. [3] (EWL for short), the classical pure strategies C and D are assigned two basic vectors $|0\rangle$ and $|1\rangle$ respectively, in a two level Hilbert space. The state of the game is a vector in the tensor product space spanned by the basis vectors $|00\rangle$, $|01\rangle$, $|10\rangle$, $|11\rangle$, where the first and second entries in the ket refer to the players A and B respectively.

The EWL protocol starts with an initial entangled state $|\psi_i\rangle = \hat{J}|00\rangle$, where the symmetric unitary operator $\hat{J} = \exp(\mathrm{i}\frac{\gamma}{2}\hat{D}^{\otimes 2})$, $\hat{D} = \left(\begin{smallmatrix}0 & 1\\ -1 & 0\end{smallmatrix}\right)$ *entangles* the player's qubits. The *entanglement factor* γ varies in the $[0, \gamma = \pi/2]$, tuning the degree of entanglement. The initial state then turns out: $|\psi_i\rangle = \left(\cos\frac{\gamma}{2}, 0, 0, \mathrm{i}\sin\frac{\gamma}{2}\right)'$, and consequently the initial density matrix, becomes:

$$\rho_i = |\psi_i\rangle\langle\psi_i| = \begin{pmatrix} \cos^2\gamma/2 & 0 & 0 & -\mathrm{i}\cos\gamma/2\sin\gamma/2\\ 0 & 0 & 0 & 0\\ 0 & 0 & 0 & 0\\ \mathrm{i}\cos\gamma/2\sin\gamma/2 & 0 & 0 & \sin^2\gamma/2\end{pmatrix}. \tag{3}$$

The players perform independently their quantum strategies as local unitary operators $(\hat{U}_A, \hat{U}_B)$ in the SU(2) space. With the only exception of Section 4, we will consider here the two-parameter subset of SU(2):

$$\hat{U}(\theta, \alpha) = \begin{pmatrix} \mathrm{e}^{\mathrm{i}\alpha}\cos(\theta/2) & \sin(\theta/2)\\ -\sin(\theta/2) & \mathrm{e}^{-\mathrm{i}\alpha}\cos(\theta/2)\end{pmatrix}, \begin{matrix}\theta \in [0, \pi]\\ \alpha \in [0, \pi/2].\end{matrix} \tag{4}$$

After the application of these strategies, the state of the game evolves to $|\psi_{f_0}\rangle = (\hat{U}_A \otimes \hat{U}_B)\hat{J}|00\rangle$. Prior to measurement, the $\hat{J}^\dagger$ gate is applied and the state of the game becomes $|\psi_f\rangle = \hat{J}^\dagger(\hat{U}_A \otimes \hat{U}_B)\hat{J}|00\rangle$. This follows a pair of Stern–Gerlach type detectors for measurement. As a result, the elements of $\mathbf{\Pi} = \binom{\rho_{11}\ \ \rho_{22}}{\rho_{33}\ \ \rho_{44}}$ are obtained from the diagonal of the final density matrix (5).

$$\rho_f = |\psi_f\rangle\langle\psi_f| = \hat{J}^\dagger(\hat{U}_A \otimes \hat{U}_B)\rho_i(\hat{U}_A \otimes \hat{U}_B)^\dagger\hat{J}. \tag{5}$$

If $\alpha_A = \alpha_B = 0$, or if $\gamma = 0$, Π factorizes as in the *classical* uncorrelated game (1) with $x = \cos^2\theta_A/2, y = \cos^2\theta_B/2$. In the classic context, middle-levels of θ lead to a uniform probability distribution Π, so that in the BOS game: $p_{\male} = p_{\female} = (R+\varrho)/4$. With middle-level election of the parameters it is: $\pi_{11} = \frac{1}{4}\cos^2\gamma, \pi_{22} = (1+\sin\gamma)^2/4$, so that $p_{\female} > p_{\male}$. Thus, in this sense the EWL protocol is biased towards the female player in the BOS game [4].

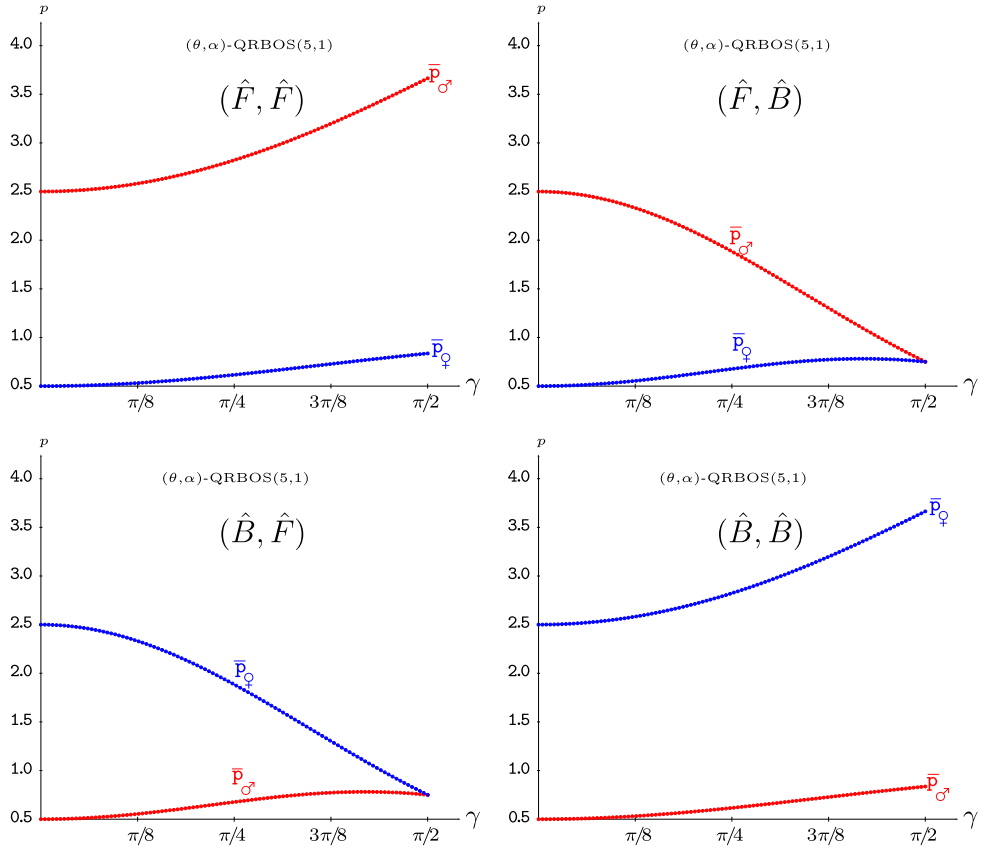

Fig. 1. Payoffs of the pure strategies in a (5,1)-QRBOS with variable entanglement factor γ at $r = \pi/4$. Top-Left: $(\hat{F},\hat{F})$, Top-Right: $(\hat{F},\hat{B})$, Bottom-Left: $(\hat{B},\hat{F})$, Bottom-Right: $(\hat{B},\hat{B})$.

1.3. Quantum relativistic games

In the Quantum-Relativistic games we deal with, in addition to the prerogatives of the previous Section 1.2, we also assume that the player A (or ♂) moves with a uniform acceleration a, and the player B (or ♀) remains stationary [5,6]. In this scenario, as a result of the so called the Unruh effect [7–9], the density matrix (3) becomes:

$$\rho_{B,I} = \begin{pmatrix} \cos^2\frac{\gamma}{2}\cos^2 r & 0 & 0 & -i\cos\frac{\gamma}{2}\sin\frac{\gamma}{2}\cos r \\ 0 & \cos^2\frac{\gamma}{2}\sin^2 r & 0 & 0 \\ 0 & 0 & 0 & 0 \\ i\cos\frac{\gamma}{2}\sin\frac{\gamma}{2}\cos r & 0 & 0 & \sin^2\frac{\gamma}{2} \end{pmatrix} \tag{6}$$

where the parameter $r \in [0, \pi/4]$ gathers the effect of the acceleration $a \in [0, \infty]$.

The probability distribution Π for $\gamma = 0$ and arbitrary r may be found in [7], where it can be checked that the equalization of the θ parameter values, so $x = y = 1/2$, leads to the equalization of the probabilities in $\Pi(\gamma = 0)$ regardless r. If both players use pure strategies, i.e., $x \in \{0, 1\},\ y \in \{0, 1\}$, $\Pi(\gamma = 0)$ gets simple forms. In particular, $\Pi^{FF} = \begin{pmatrix} \cos^2 r & \sin^2 r \\ 0 & 0 \end{pmatrix}$. Π^{FB} is obtained permuting the columns of Π^{FF}, Π^{BF} permuting the rows of Π^{FF}, and Π^{BB} permuting the rows and the columns of Π^{FF}. As a result, in the QRBOS [10,11] it is: $p_{♂} > p_{♀}$ if (F, F) or (F, B), and $p_{♂} < p_{♀}$ if (B, F) or (B, B).

The probability distribution for mutual F and arbitrary γ and r parameters is given in (7). As with $\gamma = 0$, permuting the columns, the rows, and the rows and columns of Π^{FF}, generate Π^{FB}, Π^{BF}, and Π^{BB}. As a result: $p_{♂} < p_{♀}$ if (F, F) or (F, B), and $p_{♂} > p_{♀}$ if (B, F) or (B, B).

$$\Pi^{FF} = \begin{pmatrix} \left(\cos^2\frac{\gamma}{2}\cos r + \sin^2\frac{\gamma}{2}\right)^2 & \cos^4\frac{\gamma}{2}\sin^2 r \\ \frac{1}{4}\sin^2\gamma\sin^2 r & \frac{1}{4}\sin^2\gamma(1-\cos r)^2 \end{pmatrix}. \tag{7}$$

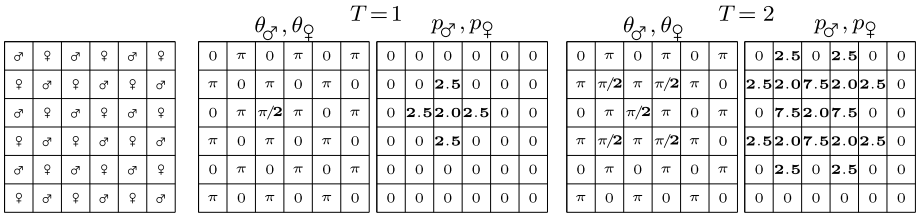

Fig. 2. The spatial BOS scenario. Far left: The ♂, ♀ chessboard. Centre: A classic inertial example where every player play its preferred choice, except the male player located in the (3,4) cell. Far right: Parameter and payoff patterns at $T = 2$.

Fig. 1 shows the payoffs of the pure strategies in the QRBOS with (5,1) parameters at $r = \pi/4$ for variable γ. At this maximum level of r it is $\Pi^{FF}_{\gamma=0} = \Pi^{FB}_{\gamma=0} = \frac{1}{2}\begin{pmatrix}1 & 1\\ 0 & 0\end{pmatrix}$, and $\Pi^{BF}_{\gamma=0} = \Pi^{BB}_{\gamma=0} = \frac{1}{2}\begin{pmatrix}0 & 0\\ 1 & 1\end{pmatrix}$, and consequently: $p^{FF}_{♂} = p^{FB}_{♂} = p^{BF}_{♀} = p^{BB}_{♀} = \frac{R}{2} = 2.5$, $p^{FF}_{♀} = p^{FB}_{♀} = p^{BF}_{♂} = p^{BB}_{♂} = \frac{\varrho}{2} = 0.5$.

Let us conclude this section by pointing out that constant acceleration of one player, as supposed in the theoretical setting of quantum relativistic games, is not the only way of altering the density matrix ρ. Of course there are other ways to extend ρ, such as including noisy channels. In that case, the density matrix depends on some parameters standing for the strength of noise. We plan to study the effect of noise in the QRBOS in further work.

2. The spatialized QRBOS

In the spatial version of the Quantum-Relativistic BOS (QRBOS-CA) we deal with, each player occupies a site (i, j) in a two-dimensional $N \times N$ lattice. We will consider that *males* and *females* alternate in the site occupation. Thus, both kind of players are arranged in a chessboard form, so that every player is surrounded by four partners (♀–♂, ♂–♀), and four mates (♀–♀, ♂–♂). The game is played the cellular automata (CA) manner, i.e., with uniform, local and synchronous interactions [12]. Thus, every player plays with his four adjacent partners, so that the payoff $p^{(T)}_{i,j}$ of a given individual is the sum over these four interactions. The evolution is ruled by the (deterministic) imitation of the best paid neighbour, so that in the next generation, every generic player (i, j) will adopt the parameters of his/her mate player (k, l) with the highest payoff among their mate neighbours. Fig. 2 shows a simple example in the classic inertial context where initially every player play its preferred choice ($\theta_{♂} = 0 \equiv x = 1, \theta_{♀} = \pi \equiv y = 0$), except the male player located in the (3,4) cell which plays $\theta_{♂} = \pi/2 \equiv x = 1/2$. Thus at $T = 1$ only the players adjacent to the male player located in (3,4) get non-zero payoffs. The imitation mechanism spreads $\theta_{♂} = \pi/2$ across the male cells, so that both male and female players get non-zero payoffs, with the females getting higher payoffs as her $\theta_{♀} = \pi$ choice remains unaltered.

All the simulations in this work are run in a $N = 200$ lattice with periodic boundary conditions and initial random assignment of the (θ, α, r) parameter values. The computations have been performed by a double precision Fortran code run on a mainframe. The *random_number* Fortran function has been used in randomization, making sure that the initial random assignation of the quantum and acceleration parameters remains unaltered for every choice of the entanglement parameter by means of the *random_seed* Fortran function.

Fig. 3 shows the dynamics up to $T = 100$ in simulations in the (5,1)-QRBOS-CA scenario with $\gamma = 0$ (left), $\gamma = \pi/4$ (centre), and $\gamma = \pi/2$ (right). As a result of the initial random assignment of the parameter values, it is initially in every frame: $\overline{\theta} \simeq \pi/2 = 1.570$, $\overline{\alpha} \simeq \pi/8 = 0.785$, and $\overline{r}_{♂} \simeq \pi/8 = 0.196$. With $\gamma = 0$, $\overline{r}_{♂}$ drifts to zero (i.e., to the inertial scenario), as well a both $\overline{\theta}_{♂}$ and $\overline{\theta}_{♀}$, which means that both players choose F and consequently $\overline{p}_{♂} = R = 5$, $\overline{p}_{♀} = \varrho = 1$ in the long term. The stabilization of the mean values of both α parameters in the $\gamma = 0$ scenario (where the $\alpha_{♂}$ and $\alpha_{♀}$ parameters are in fact irrelevant) indicates the complete stabilization of the system, once the (5,1) payoffs are fixed all around the lattice. With $\gamma = \pi/4$, $\overline{r}_{♂}$ holds a non-zero value (though at a small value), both $\overline{\theta}_{♂}$ and $\overline{\theta}_{♀}$ reach similar values, whereas $\overline{\theta}_{♀}$ outperforms $\overline{\theta}_{♂}$. With $\gamma = \pi/2$, the dynamics of the $\overline{\alpha}$ and $\overline{\theta}$ parameters are similar to those with $\gamma = \pi/4$, whereas $\overline{r}_{♂}$ reaches a value that is higher than the low one show with $\gamma = \pi/4$. It is remarkable, that the just commented tendencies heavily emerge from the very beginning as a rule, despite the full range of parameters initially accessible in the CA local interactions. Please, note that the simulations in Fig. 3 are shown up to $T = 100$, not up to $T = 200$ as implemented here to make sure that the dynamics achieve stable states. In this way, the fluctuations and apparent lack of convergence observable in some parameters in the centre and right frames of Fig. 3 vanish long before $T = 200$.

Fig. 3 shows also the dynamics of the mean-field payoffs (p^*) achieved in a single hypothetical two-person game with players adopting the mean parameters appearing in the spatial dynamic simulation. Namely, with $r_{♂} = \overline{r}_{♂}$ and,

$$U^*_{♂} = \begin{pmatrix} e^{i\overline{\alpha}_{♂}} \cos\overline{\omega}_{♂} & \sin\overline{\omega}_{♂} \\ -\sin\overline{\omega}_{♂} & e^{-i\overline{\alpha}_{♂}} \cos\overline{\omega}_{♂} \end{pmatrix}, \qquad U^*_{♀} = \begin{pmatrix} e^{i\overline{\alpha}_{♀}} \cos\overline{\omega}_{♀} & \sin\overline{\omega}_{♀} \\ -\sin\overline{\omega}_{♀} & e^{-i\overline{\alpha}_{♀}} \cos\overline{\omega}_{♀} \end{pmatrix}. \tag{8}$$

Fig. 4 shows the patterns in the $\gamma = \pi/2$ scenario of Fig. 3, where increasing grey levels indicate increasing values. From left to right: (θ, α, r) parameter patterns, and payoff pattern. The parameter patterns in Fig. 4 show a kind of maze-like

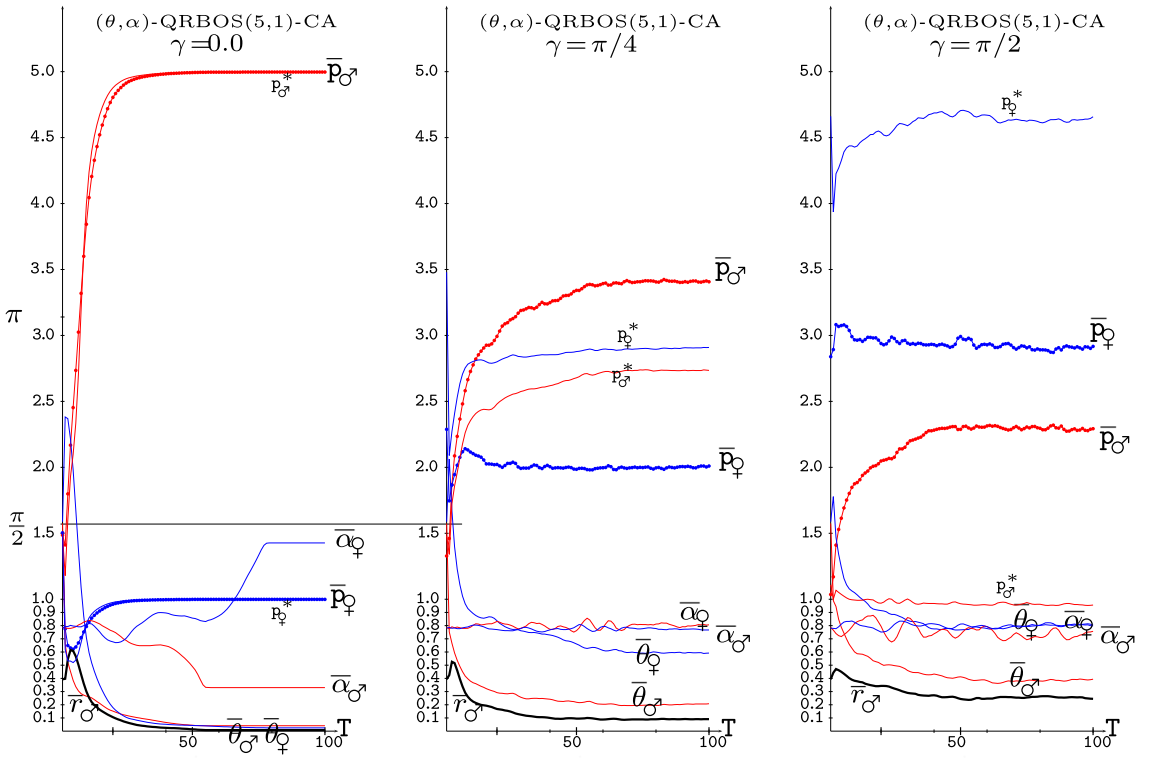

Fig. 3. Dynamics up to $T = 100$ in three simulations in the (5,1)-QRBOS-CA. Left: $\gamma = 0$, Centre: $\gamma = \pi/4$, Right: $\gamma = \pi/2$.

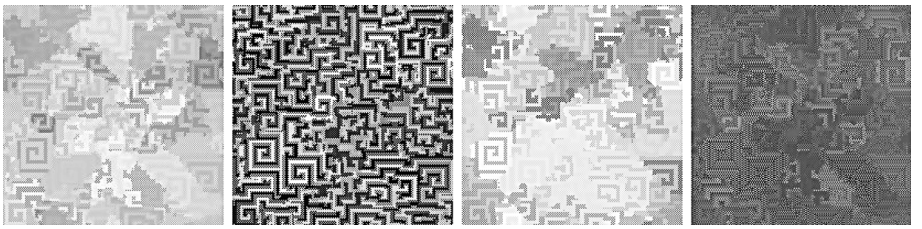

Fig. 4. Patterns at $T = 200$ in a simulation in the $\gamma = \pi/2$ scenario of Fig. 3. From left to right: (θ, α, r) parameter patterns, and payoff pattern. Increasing grey levels indicate increasing values.

aspect, particularly crisp in the α pattern, a kind of spatial heterogeneity that explains why the mean-field estimations of the payoffs differ from the actual ones in the $\gamma \neq 0$ scenarios of Fig. 3. The divergence of the mean-field payoffs and the actual ones becomes apparent from the initial iterations in the right frame ($\gamma = \pi/2$) of Fig. 3, leading to notably distant p^* and $\overline{p}$ values in the long term. The actual *vs*. mean-field divergence in the central frame of Fig. 3, i.e., with $\gamma = \pi/4$, becomes apparent latter compared to the $\gamma = \pi/2$ case. The mean-field payoff estimates of both player types with $\gamma = \pi/4$ (central frame) slowly approach, so that at $T = 200$ their values equalize, as becomes apparent in 5, but in Fig. 4 they are still different at $T = 100$.

Fig. 5 deals with the results obtained at $T = 200$ in five simulations (five different initial random assignment of the (θ, α, r) parameter values) of a (5,1)-QRBOS-CA with variable entanglement factor γ. Fig. 5 shows in its right frame the mean parameter values across the lattice and in its left frame the mean payoffs across the lattice ($\overline{p}$) and the mean-field payoffs (p^*) of both player types. The results with $\gamma = 0$, $\gamma = \pi/4$ and $\gamma = \pi/2$ in Fig. 5 are foreseeable from Fig. 3. Thus, regarding the payoffs, with $\gamma = 0$ (with no spatial effects): $\overline{p}_{\male} = p^*_{\male} = R = 5 > \overline{p}_{\female} = p^*_{\female} = \varrho = 1$; with $\gamma = \pi/4$: $\overline{p}_{\male} > p^*_{\male} = p^*_{\female} > \overline{p}_{\female}$; and with $\gamma = \pi/2$: $p^*_{\female} > \overline{p}_{\female} > \overline{p}_{\male} > p^*_{\male}$. The main conclusion derived from the payoff frame (left) in Fig. 5 is that the mean payoff ($\overline{p}$) of the accelerated male overrates the inertial female if $\gamma < 3\pi/8$, whereas the inertial female overrates the accelerated male if $\gamma > 3\pi/8$. It seems that the bias towards the female player mentioned in Section 1.2 prevails in contests with very high entanglement. The mean-field payoff approaches (p^*) also react to the increase of γ in this way, but with payoff equalization achieved before, at $\gamma = \pi/4$. The right frame of Fig. 5 shows that

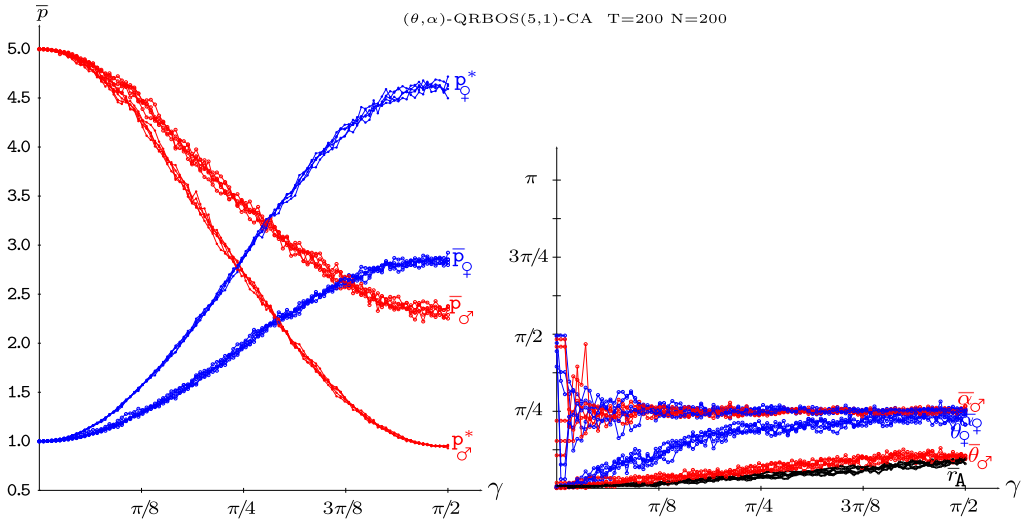

Fig. 5. Five simulations at $T = 200$ of a (5,1)-QRBOS-CA with variable entanglement factor γ. Left: Actual mean payoffs across the lattice $\overline{p}$, and mean-field payoffs p^*. Right: Mean parameter values across the lattice in the simulations.

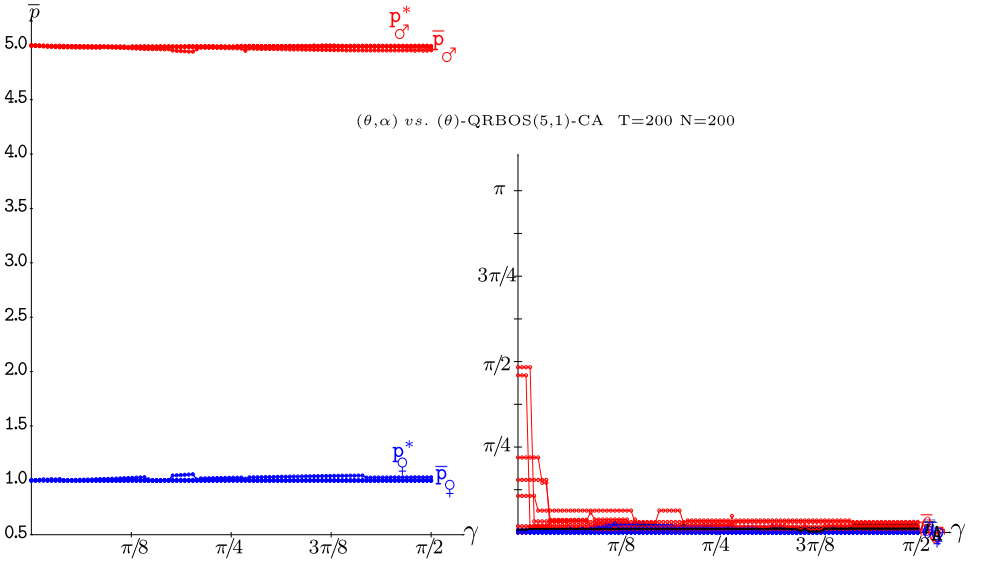

Fig. 6. Five simulations at $T = 200$ of an unfair quantum accelerated (θ, α)-male player (red) versus inertial θ-female player (blue) (5,1)-QRBOS-CA with variable entanglement factor γ. Left: Actual mean payoffs across the lattice $\overline{p}$, and mean-field payoffs p^*. Right: Mean parameter values across the lattice. (For interpretation of the references to colour in this figure legend, the reader is referred to the web version of this article.)

both $\overline{r}_{\male}$ and $\overline{\theta}_{\male}$ slowly grow as γ increase, whereas $\overline{\theta}_{\female}$ grows much faster, reaching $\overline{\theta}_{\female} \simeq \pi/4$ at $\gamma = \pi/2$. Both $\overline{\alpha}_{\male}$ and $\overline{\alpha}_{\female}$ oscillate nearly $\pi/4$ after a noisy regime for low values of γ.

3. Unfair contests

In *unfair* contexts, a type of players is restricted to classical strategies $\tilde{U}(\theta, 0)$, whereas the other type of players may use quantum $\hat{U}(\theta, \alpha)$ ones [13].

Fig. 6 deals with five simulations of an accelerated (θ, α)-male player (red) versus an inertial θ-female player (blue) in a (5,1)-QRBOS-CA with variable entanglement factor γ. Its left frame shows that the (θ, α)-male player fully overrates the θ-female player regardless γ. This is so with no spatial effects as the mean-field payoff approaches (p^*) fully coincide with the actual mean payoffs ($\overline{p}$) for both player types. The right frame of Fig. 6 shows how every parameter, including $\overline{r}_{\male}$, plummets to zero in the long term, so that $\pi_{11} = 1$ and consequently $p_{\male} = R = 5$ and $p_{\female} = \varrho = 1$.

Fig. 7 deals with five simulations of an accelerated θ-male player (red) versus an inertial (θ, α)-female player (blue) in a (5,1)-QRBOS-CA with variable γ. Thus, the scenario of Fig. 6 but with reversed unfairness, now favouring the female player.

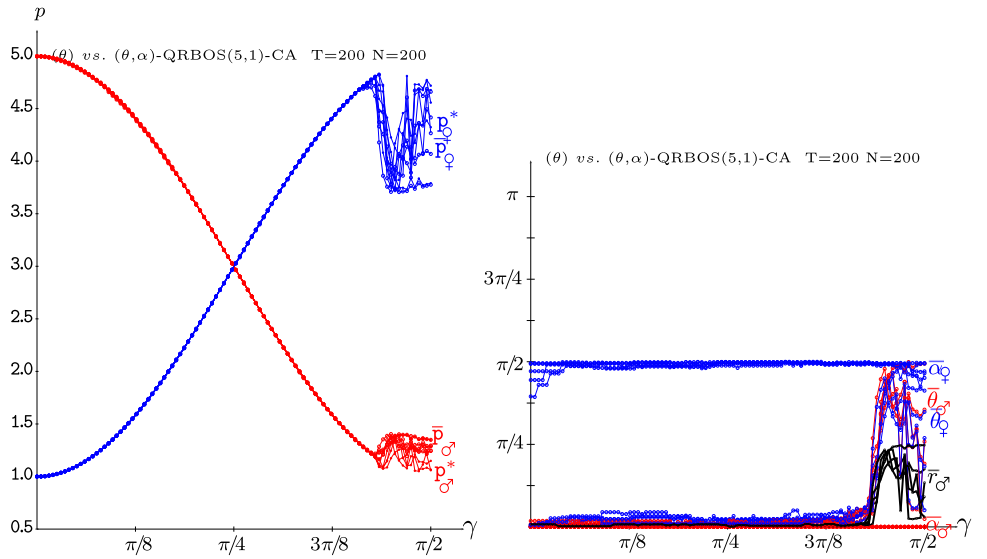

Fig. 7. Five simulations at $T = 200$ of an unfair accelerated θ-male player (red) versus inertial (θ, α)-female player (blue) (5,1)-QRBOS-CA with variable entanglement factor γ. Left: Actual mean payoffs $\overline{p}$, and mean-field payoffs p^*. Right: Mean parameter values across the lattice. (For interpretation of the references to colour in this figure legend, the reader is referred to the web version of this article.)

The left frame of Fig. 7 shows that the *favoured* player, i.e., the female, overrates the male beyond $\gamma = \pi/4$, but that, fairly contrary to expectation after Fig. 6, the player with only the θ parameter available, i.e., the male, overrates the female below $\gamma = \pi/4$. In the same vein as in the simulations of Fig. 6, no spatial effects emerge in the simulations of Fig. 7 as $p^* \simeq \overline{p}$ for both player types. The right frame of Fig. 7 shows that the $\alpha_{♀}$ parameter keeps $\overline{\alpha}_{♀} \simeq \pi/2$ regardless γ in the long term, whereas the remaining parameters, including $\overline{r}_{♂}$, plummets to zero up to γ nearly the midpoint of the $[3\pi/8, \pi/2]$ interval, referred to as γ^* in what follows. We do not have any explanation to justify the odd behaviour detected in Fig. 7 for high gamma, particularly, in what respect to the *reappearance* of the r parameter. A similar phenomenon was found when dealing with the PD game (Fig. 8 in [7]). Any attempt to explain it is postponed to a further study dealing with the effect of quantum noise. With $\gamma > \gamma^*$ the parameters show a rather erratic behaviour that is reflected in the payoffs values in the left frame. But with $\gamma < \gamma^*$, where $\overline{r}_{♂} \simeq \overline{\theta}_{♂} \simeq \overline{\theta}_{♀} \simeq 0$, the mean-field estimation leads to a diagonal Π, i.e., non-factorizable, with $\pi_{22} = \sin^2(\alpha_{♂} + \alpha_{♀}) \sin^2\gamma$, $\pi_{11} = 1 - \pi_{22}$; if additionally $(\alpha_{♂} + \alpha_{♀}) = \pi/2$ it turns out $\pi_{11} = \cos^2\gamma$, $\pi_{22} = \sin^2\gamma$, so that $p_{♂}(\gamma) = R\cos^2\gamma + \varrho \sin^2\gamma$, $p_{♀}(\gamma) = \varrho\cos^2\gamma + R\sin^2\gamma$. The latter formulas correspond to the *scissors*-like shape of the payoffs before γ^* in the left frame of Fig. 7. In particular, $p_{♂}(0) = R = 5$, $p_{♀}(0) = \varrho = 1$; $p_{♂}(\pi/4) = p_{♀}(\pi/4) = (R + \varrho)/2 = 3$.

4. Three-parameter strategies

This section deals with the full space of strategies SU(2), operating with three parameters as given in (9), so that a new β parameter is available [14].

$$\hat{U}(\theta, \alpha\beta) = \begin{pmatrix} e^{i\alpha}\cos(\theta/2) & e^{i\beta}\sin(\theta/2) \\ -e^{-i\beta}\sin(\theta/2) & e^{-i\alpha}\cos(\theta/2) \end{pmatrix}, \begin{matrix} \theta \in [0, \pi] \\ \alpha, \beta \in [0, \pi/2]. \end{matrix} \tag{9}$$

At variance with what happens in the two-parameter inertial frame described in Section 1.2, with middle-level election of the (θ, α, β) parameters, the probabilities in $\mathbf{\Pi}$ turns out equalized regardless γ in the inertial frame [15,16].

Fig. 8 shows the results achieved in the scenario of Fig. 5, but in the three-parameter strategies model. In the graph of the actual and mean-field payoffs of this figure (left frame), the latter have been coloured as brown ($p^*_{♂}$) and green ($p^*_{♀}$) in order to discriminate them from the actual payoffs ($\overline{p}$) at higher values of γ. The graph of payoffs in Fig. 8 is reminiscent of that achieved in the scenario of Fig. 5 for low values of γ, so that the accelerated male overrates the inertial female in a decreasing manner as γ increases and the mean-field payoff estimates approach fairly well to the actual mean payoffs. But the structure of the payoff graphs for $\gamma > \pi/4$ notably differ in Fig. 8 compared to that in Fig. 5. Thus, the actual payoffs tend to equalize instead to diverge, and the mean-field estimates show an erratic behaviour instead of the crisp aspect shown not only in Fig. 5 but also in the unfair contests simulations.

The graphs of the mean parameter values (right frame) in Fig. 8 indicates that the particularly high variability in the $\overline{\theta}$ parameters for $\gamma > \pi/4$ would explain that variability in the mean-field payoff estimates for high values of γ over

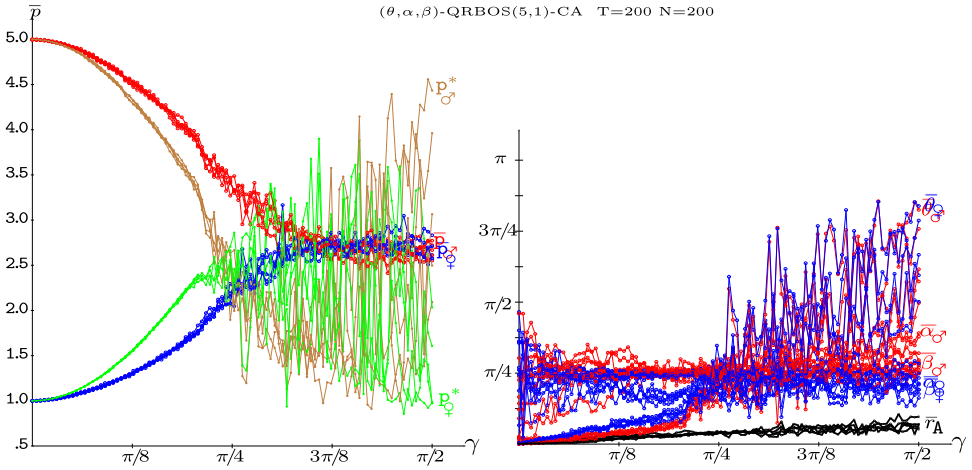

Fig. 8. Five simulations at $T = 200$ in a three-parameter (5,1)-QRBOS-CA with variable entanglement factor γ. Left: Actual mean payoffs across the lattice $\overline{p}$ (red, blue), and mean-field payoffs p^* (brown, green). Right: Mean parameter values across the lattice. (For interpretation of the references to colour in this figure legend, the reader is referred to the web version of this article.)

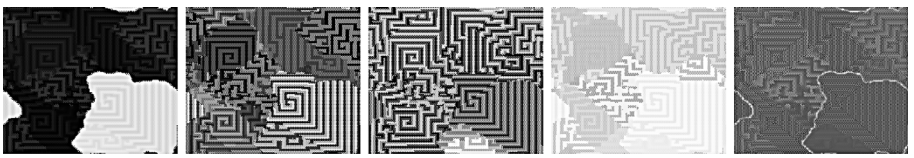

Fig. 9. Patterns at $T = 200$ in a simulation in the $\gamma = \pi/2$ scenario of Fig. 8. From left to right: $(\theta, \alpha, \beta, r)$ parameter patterns, and payoff pattern. Increasing grey levels indicate increasing values.

approximately its midpoint. Remarkably, this dramatic variability in the mean-field payoff estimates p^* does not correspond with a similar variability in the actual mean payoff $\overline{p}$ which vary in a smooth way as γ grows, pointing out to notable spatial effects, that Fig. 9 exemplifies. The $\overline{r}_{♂}$ parameter varies in Fig. 8 much as in Fig. 5, slowly growing as γ increases.

The Nash Equilibrium (NE) strategies in the noninertial QBOS frame in the full space of strategies is studied in [11]. It is concluded in [11] that the NE in the classic inertial frame based in pure strategies (Section 1.1) are still in equilibrium in the noninertial frame, albeit the payoffs of both players are notably influenced by both γ and r as quantified in (7). Apparently, in the CA-simulations of Fig. 8 the accelerated-male player manages to impose strategies favouring him, i.e., with himself choosing F, for low values of γ; in the extreme case (F,F) with $\overline{r}_{♂} = 0$ if $\gamma = 0$. Let us mention here that this advantageous result achieved for the accelerated ♂-player was not found in the 3P CA-simulations in the inertial frame reported in [17]. For high values of γ the equalization of payoffs is achieved above but near $\overline{p} = 2.5$, approximately at the same level as in the 3P CA-simulations for high γ in the inertial frame [17]. Recall that the maximum equal payoff attainable in the classic inertial frame is $p^+ = (R + \varrho)/4 = 1.5$ in the uncorrelated model and $p^+ = (R + \varrho)/2 = 3.0$ in the correlated model. Incidentally, the NE based on mixed strategies in the classic uncorrelated inertial frame gives the much lower equalized payoffs $p = Rr/(R + \varrho) = 0.833$. This payoff, as well as the strategies that induce it, are retrieved making $\gamma = r = 0$ in the non-pure strategies in NE in the quantum non-inertial frame reported in [11].

Fig. 10 deals with five simulations of an accelerated (θ, α, β)-male player (red) versus an inertial θ-female player (blue) in a (5,1)-QRBOS-CA with variable entanglement factor γ. Thus, the 3P analogue to the 2P Fig. 6. Initially, for low γ, the general appearance of the payoff curves in Fig. 10 is the same as that of the Fig. 6, so that the quantum-accelerated male player fully overrates the classic inertial female player. But before $\gamma = \pi/4$, a kind of phase transition rockets the payoff of the female players and plummets that of the male players, so that contrary to expectation, the classic inertial female player overrates the quantum-accelerated male player (this is so up to $\gamma = \pi/8$). Immediately after this episode, both types of payoffs commence to approach, so that by $\gamma = \pi/4$ they equalize at the level $\overline{p} = (R + \varrho)/2 = 3.0$. After this middle-level of γ, the quantum-accelerated male player increasingly overrates the classic female player. Spatial effects emerge only in one of the simulations with very high levels of γ in Fig. 6. The right frame of Fig. 10 indicates that $\overline{r}_{♂}$ is led to zero regardless γ in the long term (as in Fig. 6), i.e., the asymptotic scenario is that of the inertial frame.

Fig. 11 deals with five simulations of an accelerated θ-male player (red) versus an inertial (θ, α, β)-female player (blue) in a (5,1)-QRBOS-CA with variable entanglement factor γ. Thus, the 3P analogue to the 2P Fig. 7, to whom Fig. 11 fully resembles. This so in particular regarding the *scissors*-like shape of the payoffs (left frame) for not too high γ.

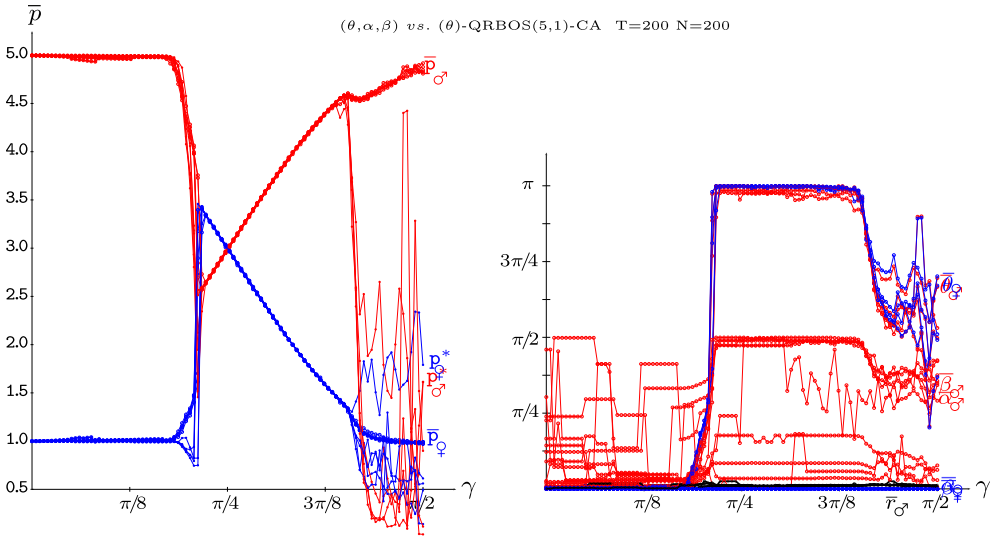

Fig. 10. Five simulations at $T = 200$ of an unfair quantum accelerated (θ, α, β)-male player (red) versus inertial θ-female player (blue) (5,1)-QRBOS-CA with variable entanglement factor γ. Left: Actual mean payoffs across the lattice $\overline{p}$, and mean-field payoffs p^*. Right: Mean parameter values across the lattice. (For interpretation of the references to colour in this figure legend, the reader is referred to the web version of this article.)

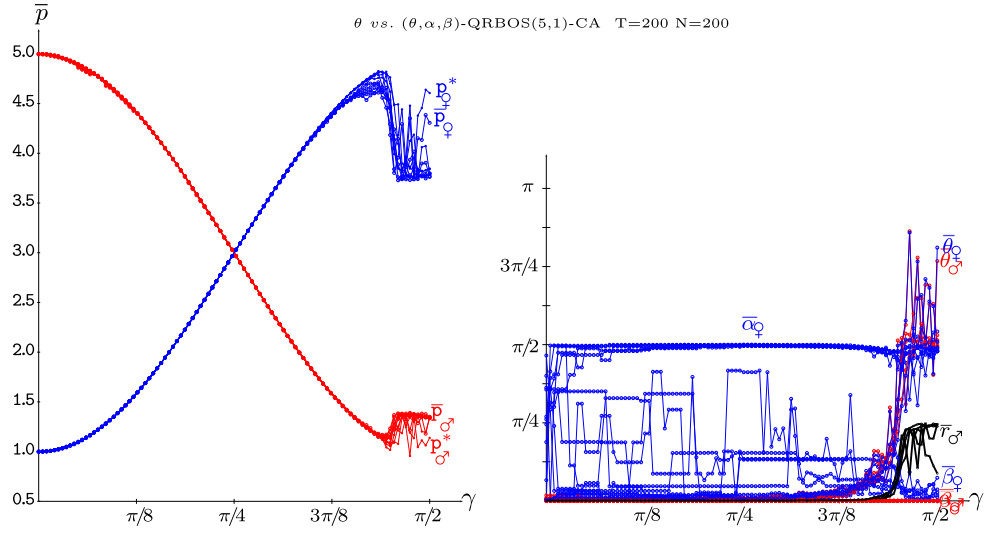

Fig. 11. Five simulations at $T = 200$ of an unfair accelerated θ-male player (red) versus inertial (θ, α, β)-female player (blue) (5,1)-QRBOS-CA with variable entanglement factor γ. Left: Actual mean payoffs $\overline{p}$, and mean-field payoffs p^*. Right: Mean parameter values across the lattice. (For interpretation of the references to colour in this figure legend, the reader is referred to the web version of this article.)

5. Conclusions and future work

A spatial formulation of the iterated quantum-relativistic battle of the sexes (QRBOS) game with arbitrary entangling degree γ is studied in this work. The game is played in the cellular automata (CA) manner, i.e., with local and synchronous players interaction. The evolution is achieved via imitation of the best paid neighbour.

As a rule, despite the full range of parameters initially accessible in the CA local interactions, the parameters of the model are quickly selected so that, after a short initial transition period, the structure of the parameter patterns, and consequently those of the payoff patterns, promptly converge to a fairly stable structure.

In the two-parameter quantum model, with contests fair in what respect to the quantum component of the game, the CA simulations evolve in the long term into parameter structures that favour the accelerated players when the entanglement factor lies below its midpoint, and to the inertial ones above the midpoint entanglement. In unfair contests, the quantum-accelerated players become fully privileged when faced with classic-inertial ones regardless γ; whereas, in unfair classic-accelerated versus quantum-inertial games, the former players overrate the later ones with entanglement under its midpoint, whereas the payoffs order reverses with entanglement over its midpoint.

In the three-parameter quantum model, the accelerated players overrate the inertial ones up to a high level of the entanglement factor, above which the payoffs of both player types tend to equalize.

Heavy spatial effects emerge in CA simulations with no negligible entanglement, particularly in fair simulations, so that mean-field payoff estimates fail to be a good approach to the actual mean payoffs.

The prisoner's dilemma has been already studied in the spatial quantum relativistic scenario in [7], but other games, particularly the Samaritan's dilemma [18] and asymmetric coordination games [19], as well as other quantization schemes [20–24] deserve particular studies in the spatial context. The effect of quantum noise [5], games with imperfect information [25,10,26] and QR games with both players accelerated are to come for scrutiny in subsequent studies.

The canonical cellular automata paradigm has been adopted here, but deviations from it may lead to more realistic models. Thus, further study is due on structurally dynamic games, games with asynchronous updating, spatial dismantling, and, last but not least, the effect of embedded tunable memory of past payoffs and parameter values [27].

One can view quantum game theory (QGT) as an exercise in pure mathematics. But the application of QGT in areas where game theory has historically attracted attention, particularly in mathematical economics, has proved to be very fruitful, given rise to a sort of *quantum econophysics* [28,29]. Nevertheless, notable difficulties, and controversies, have accompanied the attempts to apply quantum technology to the study of (potential) quantum effects in living organisms [30–32], far beyond the quantum original realm in *hard* physicochemical sciences. Some authors [33,34] speculate that – it is not inconceivable that such [quantum] 'games' are already being played at some microscopical [living] level in the real world –, but (fierce) criticism by both physicists and biologists may be also traced in the specialized literature regarding *quantum biology* [32].

Thus, likely the emergence of landmark applications of QGT lie in the future (much as it is expected with quantum computing). The current task being to provide tools that we expect will be useful in the future in order to explain *how* quantum effects that take place in a microscopic world can give rise to the macroscopic world. This article aims to contribute to this goal, by considering the added component of player's spacialization and simple interaction given by the CA paradigm. Two main reasons support the CA approach: (i) Spatialization of games, both classic and quantum, seems to be a natural way of dealing with social interactions, (ii) Building the quantum devices needed to play quantum games may not be that difficult. Just to give an example of difficulty, implementing the Shor's quantum factoring algorithm would require hundreds or thousands of entangled particles. However, in simple games such as the QRBOS studied here, only one particle per player is needed. In addition, quantum games do not require long sequences of coherent operations and hence are more likely to realize than large-scale quantum computations such as required to factor numbers large enough to be of cryptographic relevance. To summarize, we expect games to be much more widely played with quantum devices in the future, and that the CA approach will be relevant at this respect.

Acknowledgements

Part of the computations of this work were performed in EOLO, an HPC machine of the International Campus of Excellence of Moncloa, funded by the UCM and FEDER Funds. RAS contribution has been funded by the Spanish Grant MTM2015-63914-P. H. Situ's contribution has been funded by the National Natural Science Foundation of China (Grant Nos. 61502179, 61472452) and the Natural Science Foundation of Guangdong Province of China (Grant No. 2014A030310265).

References

[1] G. Owen, Game Theory, Academic Press, 1995.
[2] A. Iqbal, J.M. Chappell, D. Abbott, On the equivalence between non-factorizable mixed-strategy classical games and quantum games, Roy. Soc. Open Sci. (2016) http://dx.doi.org/10.1098/rsos.150477.
[3] J. Eisert, M. Wilkens, M. Lewenstein, Quantum games and quantum strategies, Phys. Rev. Lett. 83 (15) (1999) 3077–3080.
[4] A.P. Flitney, L.C.L. Hollenberg, Nash equilibria in quantum games with generalized two-parameter strategies, Phys. Lett. A 363 (2007) 381–388.
[5] S. Khan, M.K. Khan, Noisy relativistic quantum games in noninertial frames, Quantum Inf. Process. 12 (2) (2013) 1351–1363.
[6] S. Khan, M.K. Khan, Relativistic quantum games in noninertial frames, J. Phys. A 44 (2011) 355302.
[7] R. Alonso-Sanz, C. Carvalho, H. situ, A quantum relativistic prisoner's dilemma cellular automaton, Int. J. Theoret. Phys. 55 (10) (2016) 4310–4323.
[8] P.M. Alsing, I. Fuentes-Schuller, R.B. Mann, T.E. Tessier, Entanglement of Dirac fields in noninertial frames, Phys. Rev. A 74 (2006) 032326.
[9] S. Takagi, Vacuum noise and stress induced by uniform acceleration hawking-unruh effect in rindler manifold of arbitrary dimension, Progr. Theoret. Phys.: Suppl. 88 (1986) 1–142.
[10] H.Z. Situ, Z.M. Huang, Relativistic quantum Bayesian game under decoherence, Internat. J. Theoret. Phys. 55 (2016) 2354–2363.
[11] G. Weng, Y. Yu, A quantum battle of the sexes in noninertial frame, J. Modern Phys. 5 (2014) 9. http://dx.doi.org/10.4236/jmp.2014.59094.
[12] J.L. Schiff, Cellular Automata: A Discrete View of the World, Wiley, 2008.
[13] A.P. Flitney, D. Abbott, Advantage of a quantum player over a classical one in 2x2 quantum games, Proc. R. Soc. Lond. Ser. A Math. Phys. Eng. Sci. 459 (2038) (2003) 2463–2474.
[14] J. Eisert, M. Wilkens, Quantum Games, J. Modern Opt. 47 (14–15) (2000) 2543–2556.
[15] R. Alonso-Sanz, A quantum battle of the sexes cellular automaton, Proc. R. Soc. Lond. Ser. A Math. Phys. Eng. Sci. 468 (2012) 3370–3383.
[16] R. Alonso-Sanz, On a three-parameter quantum battle of the sexes cellular automaton, Quantum Inf. Process. 12 (5) (2013) 1835–1850.
[17] R. Alonso-Sanz, Variable entangling in a quantum battle of the sexes cellular automaton, in: ACRI-2014, in: LNCS, 8751, 2014, pp. 125–135.
[18] S.K. Özdemir, J. Shimamura, F. Morikoshi, N. Imoto, Dynamics of a discoordination game with classical and quantum correlations, Phys. Lett. A 333 (3) (2004) 218–231.
[19] H.Z. Situ, A quantum approach to play asymmetric coordination games, Quantum Inf. Process. 13 (2014) 591–599.
[20] L. Marinatto, T. Weber, A quantum approach to static games of complete information, Phys. Lett. A 272 (2000) 291–303.
[21] A. Nawaz, A.H. Toor, Dilemma and quantum battle of sexes, J. Phys. A: Math. Gen. 37 (15) (2004) 4437–4443.
[22] A. Nawaz, A.H. Toor, Generalized quantization scheme for two-person non-zero sum games, J. Phys. A: Math. Gen. 37 (42) (2004) 365305.
[23] H.Z. Situ, Two-player conflicting interest Bayesian games and Bell nonlocality, Quantum Inf. Process. 15 (2016) 137–145.

[24] H.Z. Situ, C. Zhang, F. Yu, Quantum advice enhances social optimality in three-party conflicting interest games, Quantum Inf. Comput. 16 (2016) 588–596.
[25] R. Alonso-Sanz, A cellular automaton implementation of a quantum battle of the sexes game with imperfect information, Quantum Inf. Process. 14 (10) (2015) 3639–3659.
[26] H.Z. Situ, Quantum Bayesian game with symmetric and asymmetric information, Quantum Inf. Process. 14 (2015) 1827–1840.
[27] R. Alonso-Sanz, Dynamical Systems with Memory, World Scientific Pub, 2011.
[28] H. Guo, J. Zhang, G.J. Koehler, A survey of quantum games, Decis. Support Syst. 46 (1) (2008) 318–332.
[29] C. Schinckus, A methodological call for a quantum econophysics, in: Quantum Interaction, in: LNCS, 8369, 2014, pp. 08–316.
[30] M. Alfonseca, A. Ortega, M. Cruz, S.R. Hameroff, R. Lahoz-Beltra, A model of quantum-von Neumann hybrid cellular automata: principles and simulation of quantum coherent superposition and dehoerence in cytoskeletal microtubules, Quantum Inf. Comput. 15 (1–2) (2015) 22–36.
[31] P. Ball, Physics of life: The dawn of quantum biology, Nature 474 (2011) 272–274.
[32] N. Lambert, Y.-N. Chen, Y.-C. Cheng, C.-M. Li, G.-Y. Chen, F. Nori, Quantum biology, Nat. Phys. 9 (2013) 10–18.
[33] R. Kay, N.F. Johnson, S.C. Benjamin, Evolutionary quantum game, J. Phys. A: Math. Gen. 34 (41) (2001) L547.
[34] C. Koch, K. Hepp, Quantum mechanics in the brain, Nature 440 (2006) 611–612.